J. Fluid Mech. (1981), *vol.* 113, *pp.* 23–51
Printed in Great Britain

The structure of a separating turbulent boundary layer. Part 1. Mean flow and Reynolds stresses

By ROGER L. SIMPSON, Y.-T. CHEW† AND B. G. SHIVAPRASAD

Southern Methodist University, Dallas, Texas 75275

(Received 19 August 1980 and in revised form 16 March 1981)

The problem of turbulent-boundary-layer separation due to an adverse pressure gradient is an old but still important problem in many fluid flow devices. Until recent years little quantitative experimental information was available on the flow structure downstream of separation because of the lack of proper instrumentation. The directionally sensitive laser anemometer provides the ability to measure the instantaneous flow direction and magnitude accurately.

The experimental results described here are concerned with a nominally two-dimensional, separating turbulent boundary layer for an airfoil-type flow in which the flow was accelerated and then decelerated until separation. Upstream of separation single and cross-wire hot-wire anemometer measurements are also presented. Measurements in the separated zone with a directionally sensitive laser-anemometer system were obtained for U, V, $\overline{u^2}$, $\overline{v^2}$, $-\overline{uv}$, the fraction of time that the flow moves downstream, and the fraction of time that the flow moves away from the wall.

In addition to confirming the earlier conclusions of Simpson, Strickland & Barr (1977) regarding a separating airfoil-type turbulent boundary layer, much new information about the separated region has been gathered. (1) The backflow mean velocity profile scales on the maximum negative mean velocity U_N and its distance from the wall N. A U^+ *vs.* y^+ law-of-the-wall velocity profile is not consistent with this result. (2) The turbulent velocities are comparable with the mean velocity in the backflow, although low turbulent shearing stresses are present. (3) Mixing length and eddy viscosity models are physically meaningless in the backflow and have reduced values in the outer region of the separated flow.

Downstream of fully developed separation, the mean backflow appears to be divided into three layers: a viscous layer nearest the wall that is dominated by the turbulent flow unsteadiness but with little Reynolds shearing stress effects; a rather flat intermediate layer that seems to act as an overlap region between the viscous wall and outer regions; and the outer backflow region that is really part of the large-scaled outer region flow. The Reynolds shearing stress must be modelled by relating it to the turbulence structure and not to local mean velocity gradients. The mean velocities in the backflow are the results of time averaging the large turbulent fluctuations and are not related to the source of the turbulence.

---

† Present address: Department of Mechanical and Production Engineering, University of Singapore.

1. Introduction

The problem of turbulent boundary-layer separation due to an adverse pressure gradient is an important factor in the design of many devices such as jet engines, rocket nozzles, airfoils and helicopter blades, and the design of fluidic logic systems. Until recent years little reliable quantitative experimental information was available on the flow structure downstream of separation because of the lack of proper instrumentation. As was pointed out by Simpson (1976), hot-wire anemometer and impact probes are directionally insensitive and cannot measure the backflow velocity with its changing flow direction accurately. Consequently, results from earlier studies of the backflow using these measurement techniques are suspect.

One approach to alleviate this problem is to move a hot-wire probe with a large-enough known velocity to avoid the hot-wire signal rectification that occurs with fixed probes. Coles & Wadcock (1979) used a flying hot wire or hot-wire probe mounted on the end of a rotating arm to measure two velocity components in the separated region of a two-dimensional airfoil flow at maximum lift. Although these final processed data are available as a test case for turbulence modelling, no interpretative analysis of the backflow structure is yet available from these results.

In another approach, Simpson, Strickland & Barr (1974) used a one-velocity-component directionally sensitive laser anemometer system to obtain some new features of a separating turbulent boundary layer. In addition to much turbulence structure information, it was determined: (1) that the law-of-the-wall velocity profile is apparently valid up to the beginning of the intermittent separation; (2) that the location of the beginning of intermittent separation or the upstreammost location where separation occurs intermittently is located close to where the free-stream pressure gradient begins to decrease rapidly; (3) that the normal stresses terms of the momentum and turbulent kinetic energy equations are important near separation; and (4) that the separated flow field shows some similarity of the streamwise mean velocity U, of the streamwise velocity fluctuation u', and of the fraction of time that the flow moves downstream (Simpson *et al.* 1977).

Based upon these results, modifications were made (Simpson & Collins 1978; Collins & Simpson 1978) to the boundary-layer prediction method of Bradshaw, Ferriss & Atwell (1967). However, this attempt at prediction pointed to the need to understand the relationship between the pressure-gradient relaxation and the structure of the intermittent separation region. A number of other workers, for example Pletcher (1978) and Cebeci, Khalid & Whitelaw (1979), have tried to predict this type of flow, but their assumptions about the turbulence structure near the wall are questionable. In nearly all the attempts so far, workers have extended the velocity and turbulence profile correlations that apply to attached flows to the backflow region. Even though turbulent fluctuations near the wall in the backflow region are as large as or larger than mean velocities, these predictors use a turbulence model that is tied to the mean velocity gradient. Even with adjustment of turbulence model parameters to fit one feature or another, these models do not simultaneously predict the backflow velocity profile, the streamwise pressure distribution, and the fact that length scales increase along the flow. Clearly then, a limiting factor for further improvement of the prediction of separated flows is the lack of fundamental experimental velocity and turbulence structure information with which to develop adequate

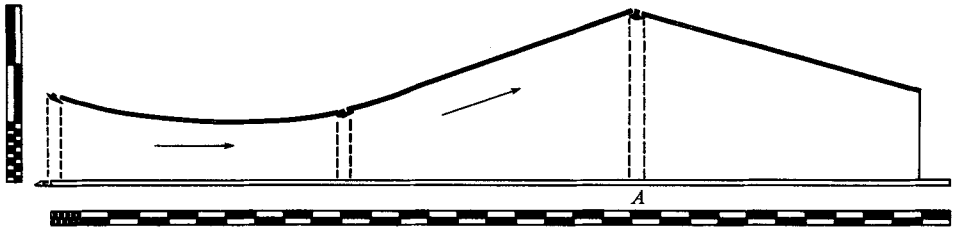

FIGURE 1. Schematic diagram of the side view of the test section. The major divisions on the scales are 10 in. Note the baffle plate upstream from the blunt leading edge on the bottom test wall and side- and upper-wall jet boundary-layer controls.

models, especially for the backflow region. Such data are presented here and in Simpson, Chew & Shivaprasad (1981) and Shiloh, Shivaprasad & Simpson (1981).

The experimental results described in this paper are concerned with a nominally two-dimensional separating turbulent boundary layer for an airfoil-type flow in which the flow was accelerated and then decelerated until separation. Upstream of separation single-wire and cross-wire hot-wire anemometer measurement results are presented. Measurements obtained in the separated zone with a directionally sensitive laser-anemometer system are presented for U, V, $\overline{u^2}$, $\overline{v^2}$, $-\overline{uv}$, the fraction of time that the flow moves downstream γ_{pu}, and fraction of time that the flow moves away from the wall γ_{pv}. The implications of these results for mixing length and eddy viscosity flow models are discussed.

2. Experimental equipment

2.1. *Basic wind tunnel*

The mainstream flow of the blown open-circuit wind tunnel is introduced into the test section after first passing through a filter, blower, a fixed-setting damper, a plenum, a section of honeycomb to remove the mean swirl of the flow, seven screens to remove much of the turbulence intensity and finally through a two-dimensional 4:1 contraction ratio nozzle further to reduce the longitudinal turbulence intensity while accelerating the flow to test speed. These same components were in an earlier version of this wind tunnel with a shorter test section (Simpson *et al.* 1977).

Figure 1 is a side-view schematic diagram of the 25 ft long, 3 ft wide test section of the wind tunnel. The upper wall is adjustable such that the free-stream velocity or pressure gradient can be adjusted. The side walls are made of floatglass. The test wall is constructed from $\frac{3}{4}$ in. thick fin-form plywood, reinforced every 11 in. with $3 \times 1\frac{1}{2} \times \frac{1}{4}$ in. cross-section steel channel.

The active boundary-layer control system, which is described by Simpson, Chew & Shivaprasad (1980), is used to eliminate preferential separation of the curved-top-wall boundary layer. Highly two-dimensional wall jets of high-velocity air are introduced at the beginning of each of the 8 ft long sections. At the latter two streamwise locations the oncoming boundary layer is partially removed by a highly two-dimensional suction system.

The inviscid core flow is uniform within 0·05 % in the spanwise direction and within 1 % in the vertical direction with a turbulence intensity of 0·1 % at 60 ft s^{-1}. The test wall boundary layer is tripped by the blunt leading edge of the plywood floor, the

height of the step from the wind tunnel contraction to the test wall being $\frac{1}{4}$ in. Smoke can be introduced uniformly into the boundary layer just upstream of this trip for use with the laser–Doppler anemometer.

2.2. *Hot-wire anemometers*

Miller-type (1976) integrated circuit hot-wire anemometers and linearizers, as modified by Simpson, Heizer & Nasburg (1979), were constructed and used. A TSI Model 1050 anemometer was used with the surface hot-wire element that is described in §2.3 below. The frequency response was flat up to 7·5 kHz for an overheat ratio of 0·7. This moderately high overheat ratio was used because Wood (1975) has shown that the range of flat frequency response is improved with a higher overheat ratio.

Standard TSI model 1274-T1.4 normal wire and model 1248-T1.5 cross-wire probes were used for boundary-layer measurements. The closest to the wall that these probes could safely make measurements was about 0·002 in. and 0·035 in., respectively. The sensing elements are 0·00015 in. diameter, 0·050 in. length platinum-plated tungsten wires.

The traversing mechanism used for the boundary-layer velocity measurements was mounted on the supporting frame for the upper wall and provided for precise positioning of the probe sensors as described by Strickland & Simpson (1973). A cathetometer was used to locate the probe sensor from the wall within an uncertainty of about $\pm$ 0·002 in. The detailed streamwise free-stream velocity distributions were obtained using the Model 1274-T1.5 probe mounted on a mobile cart that was easily positioned along the flow.

Calibrations were made in a TSI Model 1127 calibrator. There was no detectable drift of the anemometer; the function-module-type linearizers had a small amount of d.c. drift. Each linearized calibration had a low level of dispersion from a straight line, with a product moment correlation coefficient (Bragg 1974) in excess of 0·9999. The slope of each calibration varied no more than about 4 % over the life of a given probe. A standard TSI model 1015C correlator was used to obtain sum and difference values for u and v from cross-wire signals. True integrating voltmeters, each consisting of a voltage-controlled oscillator and a digital counter, were used to obtain true time-averaged results.

2.3. *Surface hot-wire skin-friction gauge*

Because a single universal calibration is valid in both laminar and turbulent flow and is insensitive to pressure gradients (Murthy & Rose 1978; Higuchi & Peake 1978), a surface hot-wire skin-friction gauge of the type used by Rubesin *et al.* (1975) was constructed and used. The basic advantages of this type of gauge are that the surface-heating-element dimension in the streamwise direction is very small and the conduction losses to a very low thermal conductivity substrate are minimized.

A 0·001 in. diameter platinum–10 % rhodium wire was mounted between 0·052 in. diameter nickel electrodes located 0·4 in. apart whose ends were flush with the flat polystyrene surface. Conduction losses to the electrodes are small since the wire length-to-diameter ratio of 400 is large. Several drops of ethyl acetate were used to dissolve the polystyrene in the vicinity of the wire and imbed it in the surface. The ends of the wire were then soldered to the electrodes. The polystyrene was mounted on a thin portable Plexiglas plate. The resulting surface was sanded and polished flat

and smooth before the wire was mounted. This plate allows a single element to be moved to various measurement locations with a minimum of flow disturbance. The element is sufficiently downstream of the end of the small ramp and sufficiently upstream of the trailing edge to avoid sensing local disturbances generated by the plate. A 0·001 in. diameter platinum and platinum–10% rhodium thermocouple was mounted $\frac{3}{32}$ in. downstream of the hot-wire element.

Rubesin *et al.* found that overheat temperatures of at least 80 °F were needed to make the heat loss from a wire proportional to its temperature rise, or $E^2/R\Delta T$ a constant. Higuchi & Peake (1978) found that overheats greater than 176 °F caused the wire to melt the substrate and separate from the surface. Here the cold resistance at 77 °F was 3·70 Ω and 0·5 Ω overheat resistance was used, so, with a temperature coefficient of resistivity of $0{\cdot}89 \times 10^{-3}$ °F^{-1}, ΔT was 152 °F. The wire was not observed to separate from the surface.

A simple stainless-steel cone with 0·5° angle between the cone and the plate surface was constructed for calibration of this gauge. A brass housing held the cone in place on the plate. The hot wire was aligned with a radial line from the cone apex. The velocity gradient at the plate surface was independent of the radial position since the cone surface velocity, ωr, and the spacing between the cone and the plate, $r \tan 0{\cdot}5°$, each vary linearly with the radius. Because the maximum surface velocity gradient of interest was about $9{\cdot}6 \times 10^4$ s^{-1}, a high-speed grinder motor (26000 r.p.m.) and a Variac power control were used to produce 600 r.p.m. $< f <$ 8000 r.p.m. A vinyl-tubing flexible connector was used between the cone shaft and the grinder to minimize misalignment. The angular speed f was measured by reflecting a light beam from the hexagonal grinder chuck nut into a photomultiplier tube and using a digital counter to measure the signal pulse rate f_p, from which we found $f = \frac{1}{6}f_p$. Heating of the calibrator flow occurred above 8000 r.p.m. due to substantial frictional heating in the steel–brass bearing. Since the air temperature was measured with the thermocouple, corrections could be made. After calibration, a Miller-type (1976) exponential electronic linearizer was used to linearize the bridge output voltage.

2.4. *Laser anemometer and signal processing*

The laser anemometer used in these experiments is described in some detail by Simpson & Chew (1979). In essence this is a two-velocity-component (U, V) directionally sensitive fringe-type system that has been used in earlier work (Simpson *et al.* 1977). The unshifted and 25 MHz Bragg-cell-shifted beams lie in an almost horizontal plane and measure the streamwise velocity with vertical fringes. The unshifted and 15 MHz Bragg-cell-shifted beams lie in a vertical plane and measure ($\mathscr{V} \cos 4{\cdot}4° + \mathscr{W} \sin 4{\cdot}4°$) with almost horizontal fringes. The 25 MHz and 15 MHz beams form a third fringe pattern that measures $(\mathscr{U} - \mathscr{V} \cos 4{\cdot}4° - \mathscr{W} \sin 4{\cdot}4°)/\sqrt{2}$ around 10 MHz. Since $\overline{u^2}$ and $\overline{(v \cos 4{\cdot}4° + w \sin 4{\cdot}4°)^2}$ were measured independently and $\overline{uw}$ was presumed very small, the Reynolds shearing stress $-\overline{uv}$ resulted from this measurement. Signal processing was by fast-sweep-rate sampling spectrum analysis, as described by Simpson & Barr (1975).

The 1 μm dioctal phthalate particles follow the highly turbulent oscillations found in separated regions (Simpson & Chew 1979). It should be noted that it is impossible to seed a highly turbulent flow in any prescribed manner. Highly turbulent flows are characterized by intense mixing of the flow. In this case there is also significant

entrainment of free-stream fluid into the turbulent motions. This would progressively dilute the particle concentration if only the shear flow was seeded. Instead of needless worry over prescribed particle concentration, concern has been with proper averaging of available signals as described below, with enough particles to provide a high data rate, and with sufficiently small particles to follow the flow accurately. In fact, without any seeding it was possible to obtain signals from the ambient dust. However, minimal seeding was used to produce a signal data rate of about 400/s.

Since the particle number density in a highly turbulent flow cannot be made uniform, the time between the passage of successive signal-generating particles will be unequal. This effect alone presents no particular signal-processing problem if the time intervals between successive signal bursts are small compared with $1/f_{\max}$, the time period of the highest flow oscillation frequency $f_{\max}$ to be detected, i.e. if the signal is almost continuous. One can simply treat the signal as a continuous hot-wire anemometer signal to obtain the averages

$$U = \frac{1}{T}\int_0^T \mathscr{U}(t)\,dt, \quad \overline{u^n} = \frac{1}{T}\int_0^T (\mathscr{U}(t)-U)^n\,dt, \tag{1), (2}$$

where $n = 2, 3, 4, \ldots$. When the time intervals between successive signal bursts are long compared with $1/f_{\max}$ (high signal drop-out rate) and are unequal, these equations should be used in the fashion explained below.

Firstly, let us look at the commonly used method of particle averaging for individual-particle velocity measurements. The averages are made over the number of signal bursts M obtained during the time period T:

$$U_M = \frac{\sum_{i=1}^{M} \mathscr{U}_i}{M}, \quad \overline{U_M^n} = \frac{\sum_{i=1}^{M} (\mathscr{U}_i - U_M)^2}{M}, \tag{3), (4}$$

where $n = 2, 3, 4, \ldots$. These averages are not made with respect to time and are biased unless the time intervals between signal bursts are equal. McLaughlin & Tiederman (1973) proposed a biasing correction that is based upon the idea that higher-velocity flow carries more particles through the focal volume per unit time. Thus, more of the high-velocity signal bursts will be obtained and U_M will be too high. However, high-velocity particles spend less time in the focal volume so that, in the case of sampling-spectrum-analysis signal processing, the chance of detecting a given signal burst varies as $(\mathscr{U}^2+\mathscr{V}^2+\mathscr{W}^2)^{-\frac{1}{2}}$. Thus, this effect tends to cancel the above-mentioned bias for particle averaging. Durão & Whitelaw (1975) showed that, if the Doppler bursts are randomly sampled before particle averaging, the bias effects are reduced significantly. Even so, particle averaging is not fundamentally a time average.

Consider now time-averaging of signals according to equations (1) and (2), even though the signal drop-out rate may be large. Only ergodic flows whose averaged quantities in equations (1) and (2) become independent of time for large T are considered. This restriction is also required for particle averaging. The last-sampled signal must be held by a sample-and-hold circuit until a new signal is detected for time-averaging. With exception of the instant at which a new signal is detected, the sampled-and-held voltage does not correspond to the actual instantaneous velocity. However, the voltage value at each instant corresponds to the instantaneous velocity at *some* instant during a recording time T for an ergodic flow. Since any averaging

process removes time-domain dependency, it does not matter when during the time period T that a given voltage occurs. It is unlikely that a given signal voltage will be averaged over too long a time (Simpson & Chew 1979). This method of averaging eliminates the need for the high-velocity-flow bias correction.

The mechanics of evaluating a true time average in this research made use of a velocity probability histogram $P(\mathscr{U})$ obtained with a SAICOR Model 41 Correlator and Probability Analyzer:

$$1 = \int_{-\infty}^{+\infty} P(\mathscr{U})\,d\mathscr{U}, \quad U = \int_{-\infty}^{+\infty} \mathscr{U} P(\mathscr{U})\,d\mathscr{U}, \tag{5), (6}$$

$$\overline{u^n} = \int_{-\infty}^{+\infty} (\mathscr{U} - U)^n P(\mathscr{U})\,d\mathscr{U}, \tag{7}$$

where $n = 2, 3, 4, \ldots$. The histogram $P(\mathscr{U})$ is constructed by sampling the $\mathscr{U}(t)$ sample-and-held signal at equal intervals in time Δt for the period T. Thus the histogram reflects a true time integral and the results from equations (5)–(7) will be equivalent to those from equations (1)–(2). The time interval Δt between digital samples should be no larger than the shortest time between signal bursts, otherwise some data will be lost. For example, $\Delta t = 10^{-4}$ s for about 400 new signals/s. The averaging time T was at least a half minute, so at least 12000 new data signals and 3×10^5 equal-time-interval samples were involved for one histogram. An added benefit of the histogram approach is that noise can be detected on an oscilloscope display while $P(\mathscr{U})$ is being constructed. The noise will cause the base level of $P(\mathscr{U})$ to grow. Thus, the resulting $P(\mathscr{U})$ can be corrected for noise or the discriminator level in the signal processor can be adjusted on-line and a new $P(\mathscr{U})$ constructed. The histograms were stored on digital tape and analysed by a digital computer.

These results are not believed to suffer strongly from bias errors. Firstly, there is no bias in the duration of a detected signal due to the flow velocity. In other words, the time that the highest-velocity particle spends in the focal volume is always large enough to produce a sufficiently large vertical voltage output from the spectrum analyser. Minimal particle seeding was used for the best SNR and data sample rate, so significant finite-transit-time broadening is unlikely.

Velocity-gradient broadening is not significant for any data presented here (Simpson 1976). The focal volume diameter 0·012 in. and length 0·140 in. are small compared with the boundary-layer thickness. In addition, signals from the centre of the focal volume are the most likely since the scattered signals are the most intense. Large-scaled motions, which scale on the boundary-layer thickness, appear to dominate the structure of highly turbulent flows, so strong instantaneous spatial velocity variations within the focal volume are unlikely. As shown below, these results compare favourably with hot-wire anemometer data obtained in regions where both types of measurement are valid.

3. Description of the test flow

All data were obtained at atmospheric pressure and $77 \pm \frac{1}{2}$ °F flow conditions. Figure 2 shows the free-stream velocity distributions obtained along the tunnel centre-line using the single-wire probe. This distribution was repeatable within 2·9 %

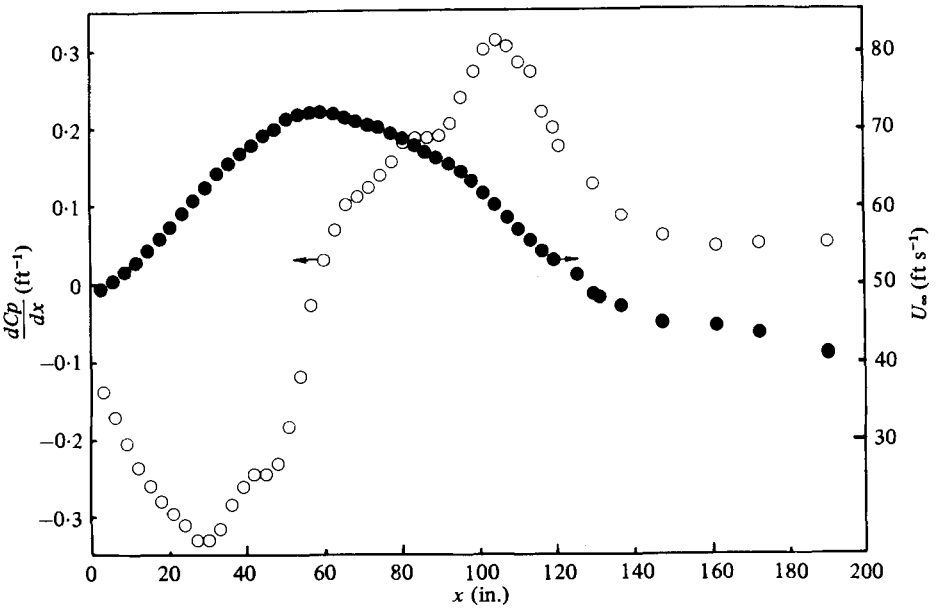

FIGURE 2. Free-stream velocity and pressure gradient distributions along the tunnel centre-line. $C_p = 2(P-P_i)/\rho U_{\infty i} = 1-(U_\infty/U_{\infty i})^2$, $U_{\infty i} = 49{\cdot}4$ ft s^{-1}.

over the duration of these experiments, which is only a little greater than the uncertainty in measuring the mean velocity with a hot-wire anemometer ($\pm 2{\cdot}4\,\%$). Figure 2 also shows the non-dimensional pressure gradient dC_p/dx along the centre-line of the test wall. Here $C_p \equiv 2(P-P_i)/\rho U_{\infty i}^2 = 1-(U_\infty/U_{\infty i})^2$, where i denotes the free-stream entrance conditions at a distance x of 3 in. A five-point local least-squares curve fit of C_p data was used at each streamwise location to determine this derivative. Just downstream of the location of the second wall-jet boundary-layer control unit (100 in.), the slope of the static pressure gradient changes sign. Near 145 in. the pressure gradient drops to an approximately constant value downstream.

To examine the two-dimensionality of the mean boundary-layer flow, smoke was introduced only in a spanwise portion of the test wall boundary layer at a given time. A sheet of laser light produced by a cylindrical lens was used to illuminate the smoke across the tunnel. Upstream of separation, negligible spanwise diffusion of the smoke was observed, indicating no gross flow three-dimensionality. Mean velocity profiles at several spanwise locations indicated that the mean velocity was two-dimensional within 1 %. Downstream of separation greater spanwise diffusion occurred, so that downstream of 170 in. no nominally two-dimensional flow remained. On the basis of these observations, the wall jet and suction boundary layer controls were adjusted to produce a nearly two-dimensional flow pattern downstream of separation. Smoke flow patterns in the side-wall and corner flows were symmetric about the channel centre-line.

The momentum integral equation provides a global test of two-dimensionality based on conservation of momentum over a large flow volume. The skin-friction terms and the summed momentum, pressure and normal stresses terms of the integrated form of the momentum integral equation differ no more than 20 %, and differ less than 16 % over 80 % of the length upstream of separation. Downstream the normal

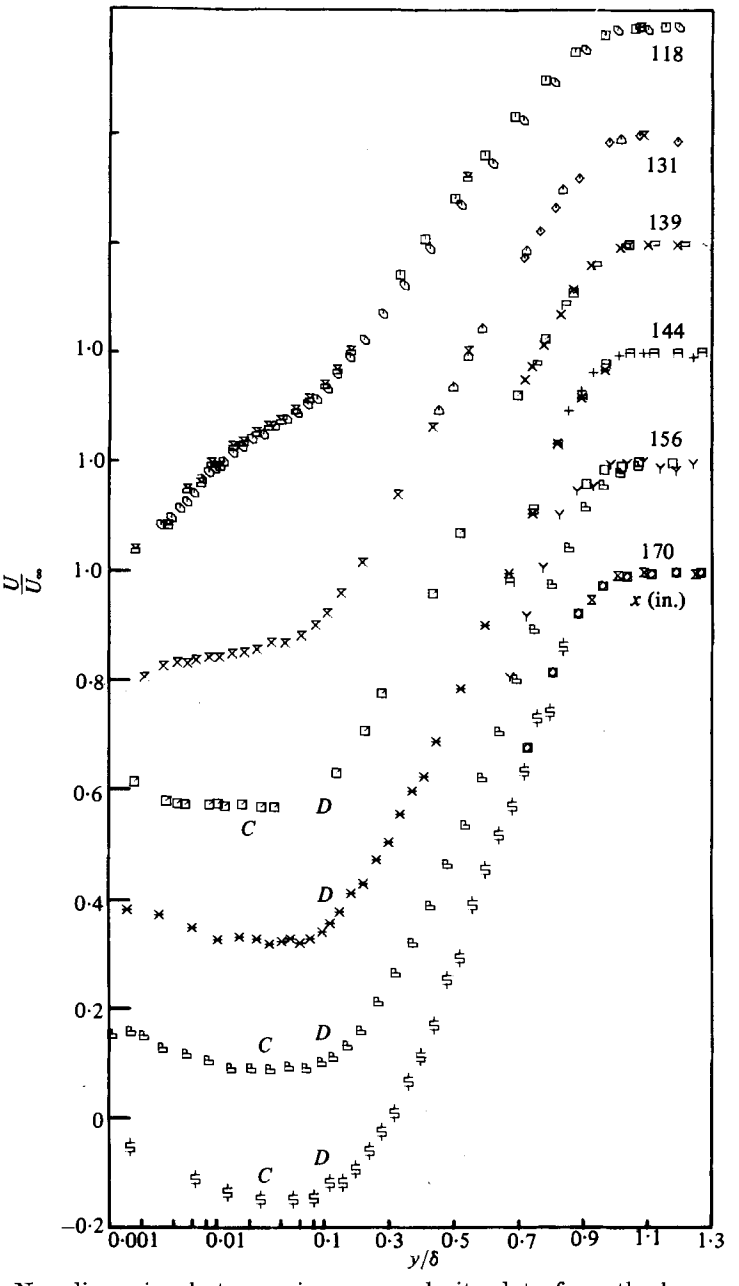

FIGURE 3. Non-dimensional streamwise mean-velocity data from the laser anemometer (near wall) and normal and X-wire hot-wire anemometers. Inflection points C and D are from Shiloh *et al.* (1981). Note the log-linear abscissa and displaced ordinates.

Normal hot-wire	$U \pm 2{\cdot}4\,\%$, $\overline{u^2} \pm 7\,\%$
Cross hot-wire (including misalignment uncertainty)	$U \pm 3{\cdot}2\,\%$, $\overline{u^2} \pm 10\,\%$, $\overline{v^2} \pm 11\,\%$, $-\overline{uv} \pm 17\,\%$
Laser anemometer	U, $V \pm 0{\cdot}2$ ft s^{-1}; $\overline{u^2}$ and $\overline{v^2}$ $\pm 4\,\%$ maximum profile value; $\overline{uv} \pm 6\,\%$ maximum profile value; $\gamma_{pu} \pm 0{\cdot}1 \exp(-U^2/2\overline{u^2})$; $\gamma_{pv} \pm 0{\cdot}1 \exp(-V^2/2\overline{v^2})$
Position from wall	$\pm 0{\cdot}002$ in.
Skin friction coefficient C_f	Ludwieg–Tillman, $\pm 6{\cdot}5\,\%$; Preston tube, $\pm 8{\cdot}5\,\%$; Surface hot-wire, $\pm 12\,\%$

TABLE 1. Estimated uncertainties of measured quantities.

stresses play a more important role, although they are not large enough to improve the momentum balance significantly.

4. Experimental results for the mean flow

4.1. *Mean-velocity profiles*

Mean-velocity profiles were obtained in the unseparated upstream boundary layer and the outer part of the separated flow using single-wire and cross-wire hot-wire anemometer probes. While some of these results are discussed here, Simpson *et al.* (1980) present them in detail and show that the upstream boundary layer behaves in a well-accepted normal fashion. The directionally sensitive laser anemometer provided velocity profiles in the separated zone and the region immediately upstream.

Figure 3 shows the streamwise mean velocity profiles for a few typical stations in the near-separation and the separated regions obtained using all three techniques. There is good agreement among these measurements, with the maximum discrepancy among them about 6–7 %. In the separated region only the laser-anemometer measurements are meaningful. Table 1 presents the experimental uncertainties for each measured quantity as determined by the method of Kline & McClintock (1953). As shown by Simpson & Chew (1979), the laser-anemometer results obtained on different days at the same location indicate a high level of data repeatability, well within the estimated experimental uncertainties.

Laser-anemometer and cross-wire anemometer results for the normal velocity component V just upstream of separation and in the separated region are in good agreement wherever the cross-wire results are valid. However, as shown in table 1, there is a fairly large uncertainty in the cross-wire result, mainly because of the uncertainty of the probe orientation with respect to the test wall. The laser-anemometer results are therefore more reliable. V grows progressively to as large as $0{\cdot}25U_\infty$ at the outer shear-layer edge at 170 in.

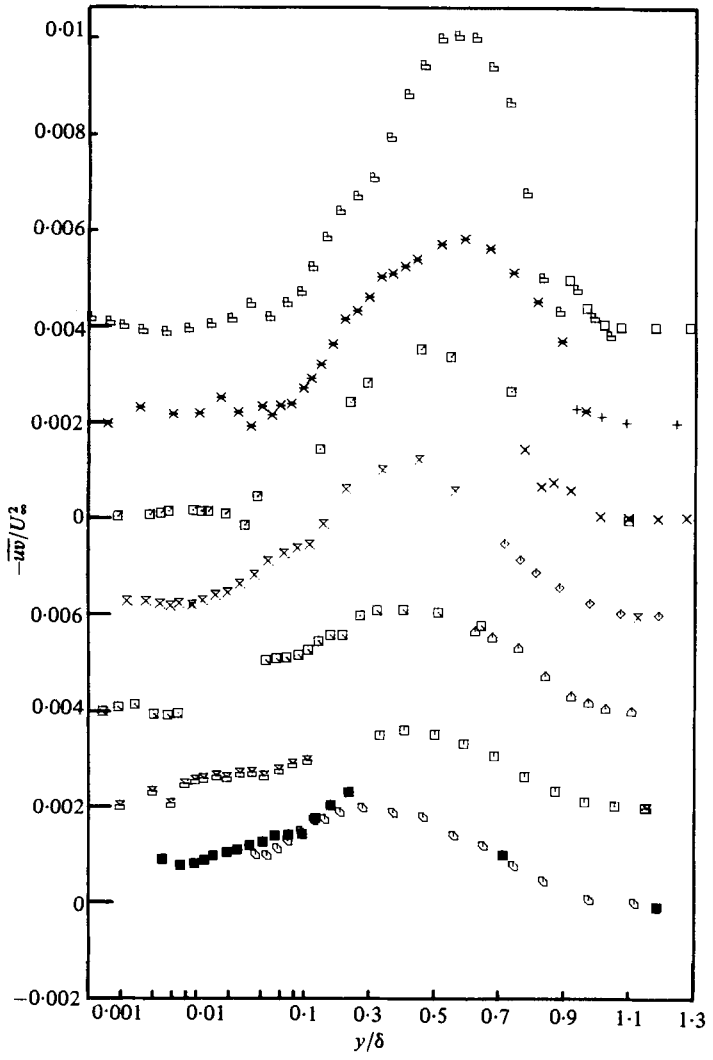

FIGURE 4. Reynolds shearing stress, $-\overline{uv}/U_\infty^2$, profiles. Note the displaced ordinates and the log-linear abscissa.

x (in.)	X-wire	LDV
112	◔	■
118	□	⊼
127	⌂	◱
131	◇	×
139	×	⊡
144	+	✱
156	□	⊏

4.2. *Turbulence quantities*

The agreement between the results for laser and cross-wire anemometer for u'/U_∞, v'/U_∞, and $-\overline{uv}/U_\infty^2$ is good with the apparent discrepancies due to the experimental uncertainties shown in table 1. The discrepancies in $-\overline{uv}/U_\infty^2$ shown in figure 4 are the greatest due to the uncertainty in orientation of the cross-wire probe

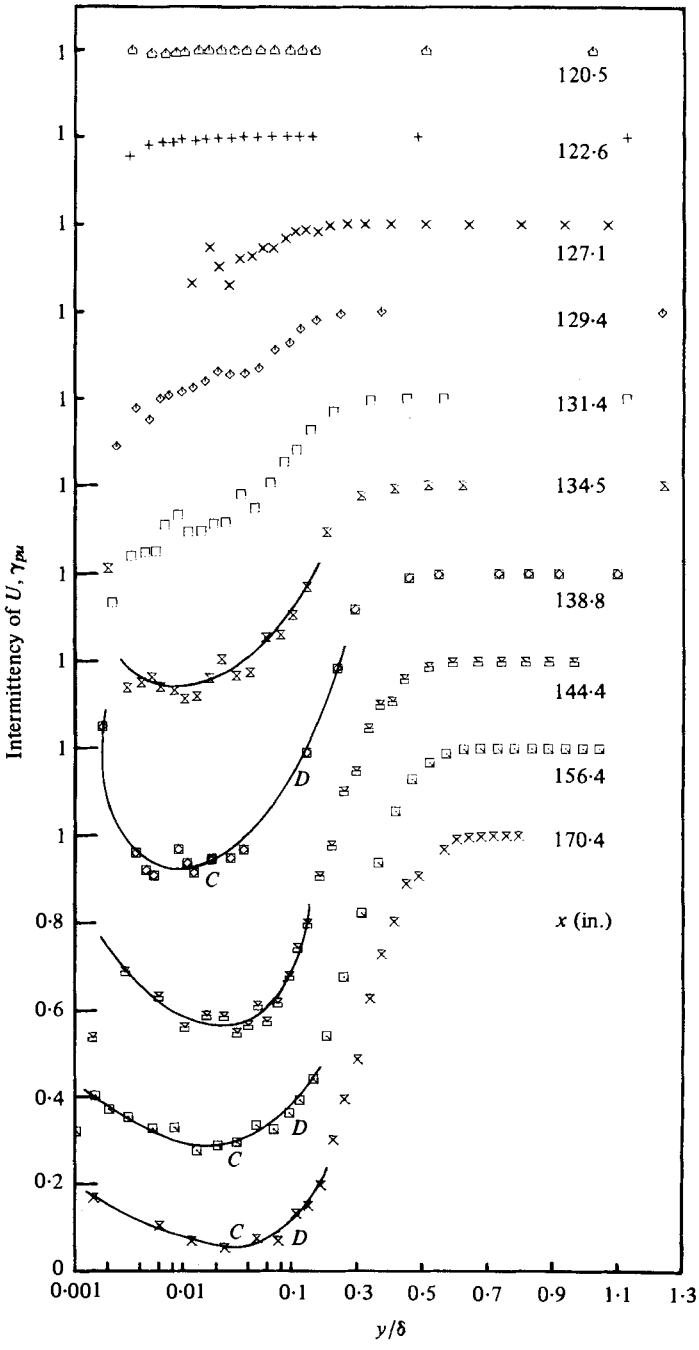

FIGURE 5. Streamwise fraction of time the flow moves downstream with the locations of inflection points C and D from Shiloh *et al.* (1981). Solid lines are for visual aid only. Note the log-linear abscissa and displaced ordinates.

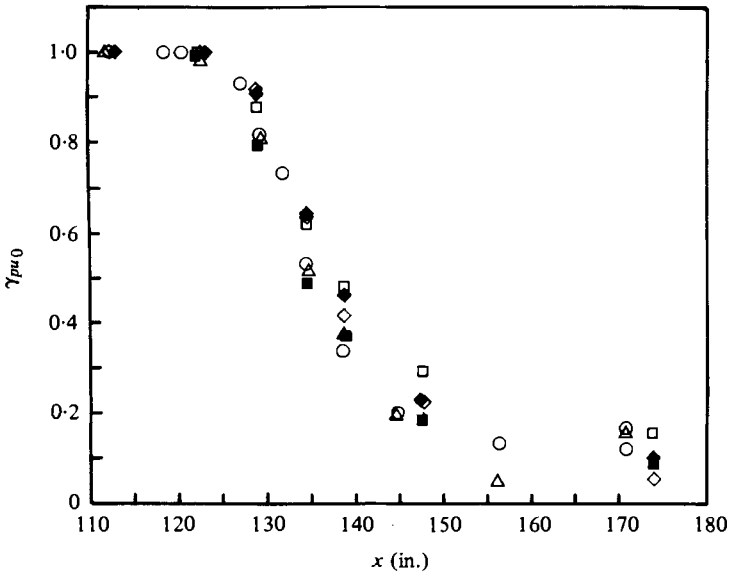

FIGURE 6. Fraction of the time that the flow 0·04 in. from the wall is in the downstream direction: ○, from LDV measurement; △, from LDV U and u' measurements. Thermal tuft with side heaters: □, position 1; ■, reversed. Thermal tuft without side heaters: ◇, position 1; ◆, reversed. From Shivaprasad & Simpson (1981).

with respect to the test wall. Since $\overline{u^2}$ and $\overline{v^2}$ are much larger than $-\overline{uv}$, only a very small misalignment is required to produce a very different $-\overline{uv}$ result. Simpson *et al.* (1980) present in detail u'/U_∞, v'/U_∞, and $-\overline{uv}/U_\infty^2$ hot-wire anemometer results for the upstream boundary layer and show that they behave in a well-accepted normal fashion.

4.3. *Upstream–downstream intermittency*

Only the directionally sensitive laser anemometer results from these measurements give information on the fraction of time that the flow moves downstream or γ_{pu}. This quantity is the fraction of the area of the velocity probability histogram that has a positive velocity. The directionally insensitive hot-wire anemometer cannot yield γ_{pu} values (Simpson 1976).

Figure 5 shows the distributions of the intermittency across the boundary layer for the region approaching separation and downstream of it. The intermittent reverse flow first starts appearing at 122·6 in. but becomes clearly observable beyond 127 in. Further downstream, the backflow intensifies and also spreads outwards from the wall. The lowest value of γ_{pu} of approximately 0·05 is reached at the last station of measurement in the separated region, where backflow extends up to about 60 % of the boundary-layer thickness. The distributions in the separated region are trough-shaped near the wall, showing that the maximum amount of reverse flow occurs slightly away from the wall. This is consistent with the velocity profile shape that shows that the highest velocity for the backflow is reached at a point slightly away from the wall. However, as shown in table 1, the uncertainty in γ_{pu} becomes large as the mean velocity approaches zero, so one cannot place too much emphasis on this coincidence. Figure 6 shows the decay of γ_{pu} near the wall, γ_{pu0}, as a function of the streamwise co-ordinate.

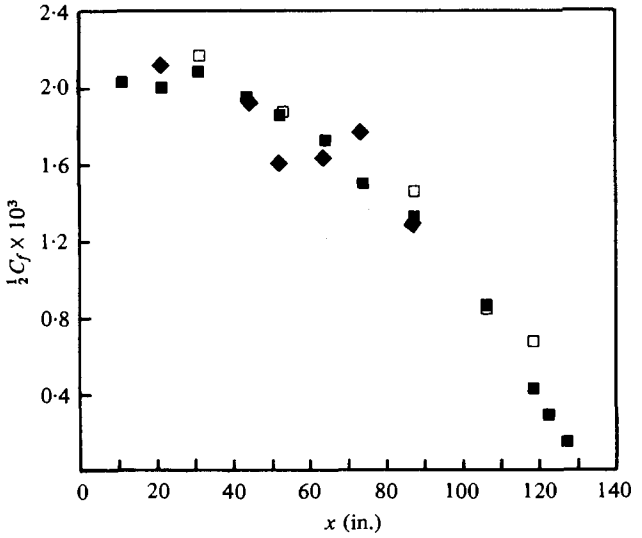

FIGURE 7. Friction factor, $\frac{1}{2}C_f$, versus x from different experimental methods: ■, Ludwig–Tillman law; □, surface hot-wire gauge; ◆, Preston tube.

x (in.)	U_∞ (ft s^{-1})	dU_∞/dx (s^{-1})	$\delta_{0\cdot99}$ (in.)	$\delta_{0\cdot995}$ (in.)	δ_1 (in.)	R_{δ_1}	H_{12}	$10^3 \times \frac{1}{2}C_f$
11·375	52·60	5·38	0·492	0·517	0·0699	1381·2	1·378	2·0350
21·750	57·80	6·48	0·574	0·615	0·0728	1570·2	1·367	2·0010
31·250	63·20	6·30	0·531	0·563	0·0707	1677·0	1·339	2·0810
44·000	68·70	4·38	0·776	0·907	0·0898	2345·9	1·323	1·9530
52·500	71·50	2·40	0·712	0·761	0·0901	2490·9	1·343	1·8620
64·250	71·60	−1·32	0·792	0·842	0·1103	2900·6	1·357	1·7240
74·250	70·00	−2·36	0·909	0·959	0·1481	3669·3	1·413	1·5030
87·500	66·80	−3·54	1·235	1·290	0·2182	5201·9	1·418	1·3300
106·310	59·30	−6·31	1·828	1·891	0·4612	8616·7	1·625	0·8590
112·375	55·90	−5·68	2·338	2·388	0·6302	9888·3	1·733	0·6982
118·500	53·10	−4·72	2·799	2·842	0·9122	11754·7	1·989	0·4469
120·500	52·15	−4·45	2·946	2·973	1·0392	12924·8	2·010	0·4219
122·625	51·30	−4·11	3·280	3·322	1·2101	13684·7	2·212	0·3030
127·125	49·50	−3·49	3·804	3·844	1·6444	14747·9	2·686	0·1418
129·375	48·75	−3·16	4·878	4·922	2·0658	19088·9	2·533	0·1680
131·875	48·10	−2·86	4·610	4·676	2·0649	16138·2	2·973	0·0884
134·500	47·40	−2·55	5·829	5·895	2·6497	19736·1	3·139	0·0646
138·750	46·45	−2·05	5·779	5·834	3·1099	17185·9	4·118	—
144·875	45·50	−1·64	6·708	6·768	4·0101	16297·7	5·404	—
156·375	44·60	−1·28	9·346	10·066	6·2550	18024·4	7·689	—
170·875	43·70	−1·21	12·518	12·841	8·3127	18664·8	9·453	—

TABLE 2. Parameters of the mean flow development.

4.4. *Skin-friction results*

Three different ways of deducing the near-wall shear-stress distribution were used: the Ludwieg–Tillman skin-friction correlation, a Preston tube, and the surface hot-wire gauge described in §2.3 above. Figure 7 shows the results from these three

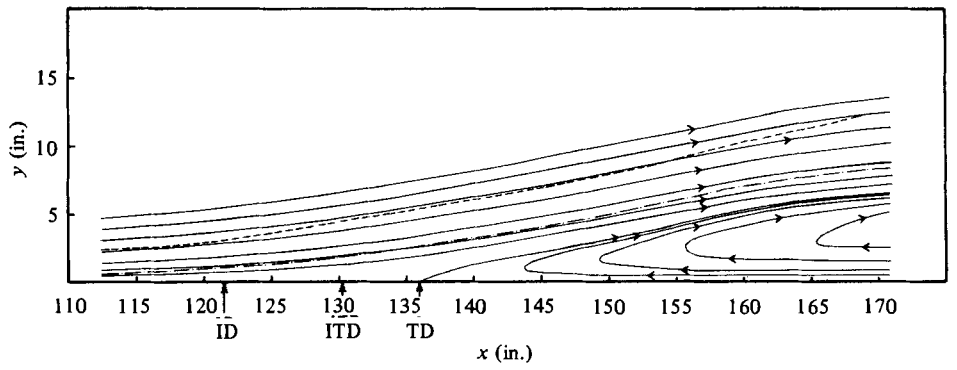

FIGURE 8. Mean streamline flow pattern in the vicinity of separation. ——, streamlines; – – – – –, boundary-layer edge; —·—, displacement thickness distribution. ID denotes *incipient detachment* with 1 % instantaneous backflow near the wall. ITD denotes *intermittent transitory detachment* with 20 % instantaneous backflow near the wall. TD denotes *transitory detachment* with 50 % instantaneous backflow near the wall.

methods, which are in agreement within the uncertainties given in table 1. Table 2 gives the Ludwieg–Tillman results.

The Preston tube and Ludwieg–Tillman methods require the existence of a universal logarithmic law-of-the-wall velocity profile. The data obtained using the surface hot-wire gauge are not dependent on the requirement of a logarithmic wall region. This suggests that the law of the wall is valid until the location where γ_{pu} is first less than one near the wall. These results are in agreement with results of Simpson *et al.* (1977).

4.5. *Data tabulation*

These data are tabulated in table 2 and in the appendix of Simpson *et al.* (1980). These data are recorded on magnetic tape in the format required for the 1980–81 AFOSR-HTTM-Stanford Conferences on Complex Turbulent Flows, a copy of which is on file in the Thermosciences Division of the Stanford University Department of Mechanical Engineering.

5. Discussion

5.1. *Mean velocity distribution*

Figure 8 shows the mean streamline pattern for the flow in the vicinity of separation. Note that in the backflow region the turbulence level is very high compared with the mean flow, so these mean streamlines do *not* represent the average pathlines for elements of fluid. As discussed by Simpson *et al.* (1981), it appears that the fluid in the backflow does not come from far downstream as the streamlines may suggest, but is supplied fairly locally.

Figure 24 in Simpson *et al.* (1980) shows that the U^+ *vs.* y^+ law-of-the-wall velocity profile holds all along the flow channel when the Ludwieg–Tillman skin friction values are used. Although no wall proximity corrections to the hot-wire data were applied in the viscous sublayer, the $U^+ = y^+$ relationship is obeyed rather well. Oka & Kostić (1972) noted that hot-wire measurements are only influenced by flow interference and conduction to the test wall for $y^+ < 4$, which explains why the present data for

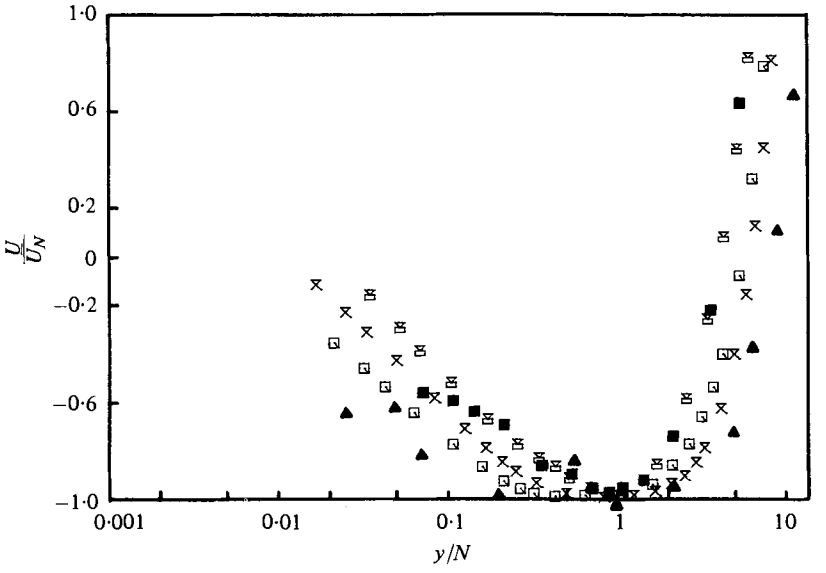

FIGURE 9. Normalized backflow mean velocity profiles: U_N and N are the maximum mean backflow velocity and its distance from the wall. ■, 138·75 in.; ⊠, 144·9; □, 156·4; ⧖, 170·9. Simpson *et al.* (1977); ▲, 165·8.

$y^+ > 4$ obey the viscous-sublayer equation so well. Upstream of the vicinity of separation, the usual logarithmic form for $y^+ > 30$ holds:

$$U^+ = \frac{1}{0{\cdot}41} \ln |y^+| + 5{\cdot}0. \tag{8}$$

Perry & Schofield (1973) proposed universal empirical correlations for the inner and outer regions of adverse-pressure-gradient boundary layers near separation. In the region near the wall, the inner-region correlation takes the usual logarithmic form of equation (8). As one proceeds downstream, the extent of the logarithmic region gradually decreases, which can also be seen from the mean velocity profiles. Their correlations apply to all types of adverse-pressure-gradient boundary layers irrespective of whether they are in equilibrium or not, but with the restriction that the ratio $(-\overline{uv})_{\max}/U_\tau^2$ must exceed 1·5. Simpson *et al.* (1977) noted that these correlations fit their data when normal stresses effects were properly accounted for.

The maximum shear-stress condition was satisfied by the present data downstream of $x = 105$ in. Simpson *et al.* (1980) show that the present data upstream of intermittent transitory detachment ($\gamma_{pu0} = 0{\cdot}20$) agree with the Perry & Schofield correlation, as modified by Simpson *et al.* (1977), within the scatter of the data originally used by Perry & Schofield.

As one can see in figure 3, there is some profile shape similarity for the backflow mean velocity downstream of 138 in. Figure 9 shows a good correlation when normalized on the maximum negative mean velocity U_N and its distance from the wall N. A slightly poorer correlation results when δ is used instead of N. The U^+ *vs.* y^+ law-of-the-wall velocity profile is not consistent with this correlation since both U_N and N increase with streamwise distance, while the law-of-the-wall length scale ν/U_τ varies

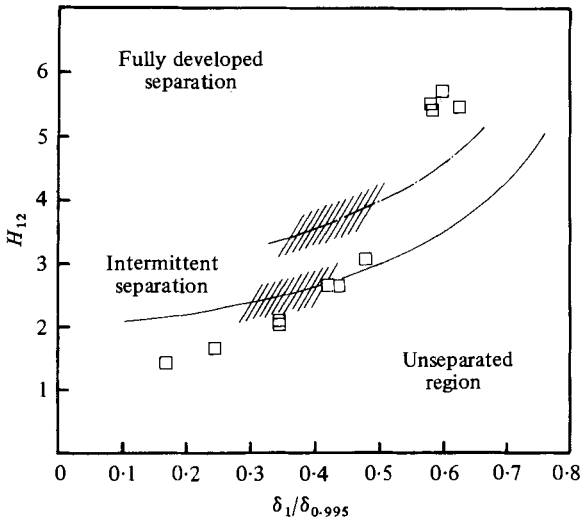

FIGURE 10. Sandborn & Liu's H_{12} *vs.* $\delta_1/\delta_{0.995}$ separation correlation: symbols, present data; ——, intermittent separation; —·—, fully developed separation.

inversely with its velocity scale U_τ. The data of Simpson *et al.* (1977) for the one available location are also shown to be in fair agreement with this correlation.

An attempt (Simpson *et al.* 1980) was made to see if the mean velocity profiles downstream of separation could be composed of the 'law-of-the-wake' (Coles & Hirst 1969) $\omega(y/\delta)$ and a similarity distribution for the remaining wall flow. There is no significant profile similarity of the remaining wall flow.

Another attempt was made to scale the wake function using the maximum backflow velocity and the free-stream velocity before subtracting it from the velocity profile. This was done as follows:

$$\frac{U}{U_\infty} = \left[\frac{U_\infty + |U_N|}{U_\infty}\right] \tfrac{1}{2}\omega(y/\delta) - \frac{|U_N|}{U_\infty} + R(y/\delta), \tag{9}$$

where $R(y/\delta)$ can be called a 'backflow' function. Furthermore, another function $B(y/\delta) = R(y/\delta)\,(U_\infty/|U_N|)$ was formed so that $B(y/\delta)$ has definite limits and is 0 at $y/\delta = 0$ and 1, respectively. Neither $R(y/\delta)$ nor $B(y/\delta)$ show any similarity or small values in the outer region. This leads one to conclude that it is not possible to describe the velocity profile in the outer region for a separated flow by the universal wake function. No universal backflow function appears to exist.

5.2. *Flow detachment and upstream–downstream intermittency*

It is well established that separation of a turbulent boundary layer does not occur at a single streamwise location but is spread over a streamwise region and involves a spectrum of states. Sandborn & Kline (1961) and Sandborn & Liu (1968) defined the limiting points of the region as the 'intermittent' and the 'fully-developed' separation points. The former indicates the onset of separation by the appearance of intermittent backflow and the latter signifies the vanishing of the mean wall shear stress.

Sandborn & Liu (1968) gave correlations between $H_{12} = \delta_1/\delta_2$ and $\delta_1/\delta_{0.995}$ to demarcate the regions of intermittent and fully developed separation. Figure 10 gives

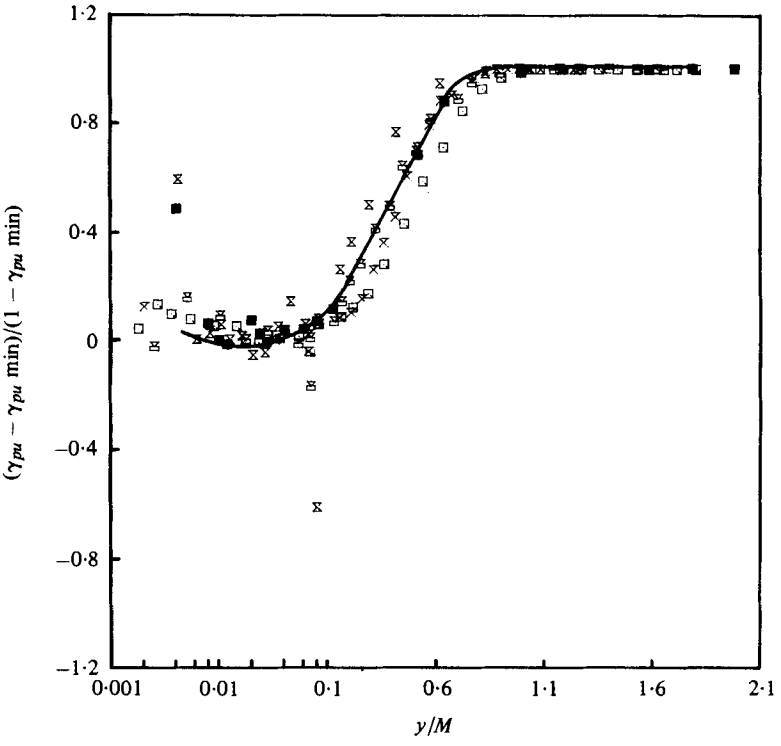

FIGURE 11. $(\gamma_{pu}-\gamma_{pu_{\min}})/(1-\gamma_{pu_{\min}})$ *vs.* y/M; $\gamma_{pu_{\min}}$ is obtained from figure 5. M is the distance from the wall to $u'_{\max}$. ——, distribution from Simpson *et al.* (1977). Data: ⧖, 134·5 in.; ■, 138·8; ⧖, 144·9; □, 156·4; ⧖, 170·9.

these correlations and the present experimental data points. According to their correlations, the present data show intermittent separation to occur at 130 in. The value of γ_{pu0} at that point is 0·81 which very nearly coincides with the value obtained by Simpson *et al.* (1977) for intermittent separation and is also in reasonable agreement with the value obtained by Sandborn & Liu. By interpolation, the fully developed separation location occurs at 140 in.

At the recent Project SQUID Colloquium on Flow Separation (Simpson 1979), it was pointed out that the term '*separation*' must mean the entire process of 'departure' or 'breakaway' or the breakdown of boundary-layer flow. An abrupt thickening of the rotational flow region next to a wall and significant values of the normal-to-wall velocity component must accompany breakaway, otherwise this region will not have any significant interaction with the free-stream flow.

A set of quantitative definitions on the detachment state near the wall were proposed: *incipient detachment* (ID) occurs with 1% instantaneous backflow; *intermittent transitory detachment* (ITD) occurs with 20% instantaneous backflow; *transitory detachment* occurs with 50% instantaneous backflow; and *detachment* occurs where $\overline{\tau_w} = 0$. Sandborn & Liu's intermittent and fully developed separation locations correspond to the intermittent transitory detachment and detachment locations, respectively.

Figure 8 shows the locations of incipient detachment, intermittent transitory detachment, and transitory detachment for the present flow obtained from figure 6.

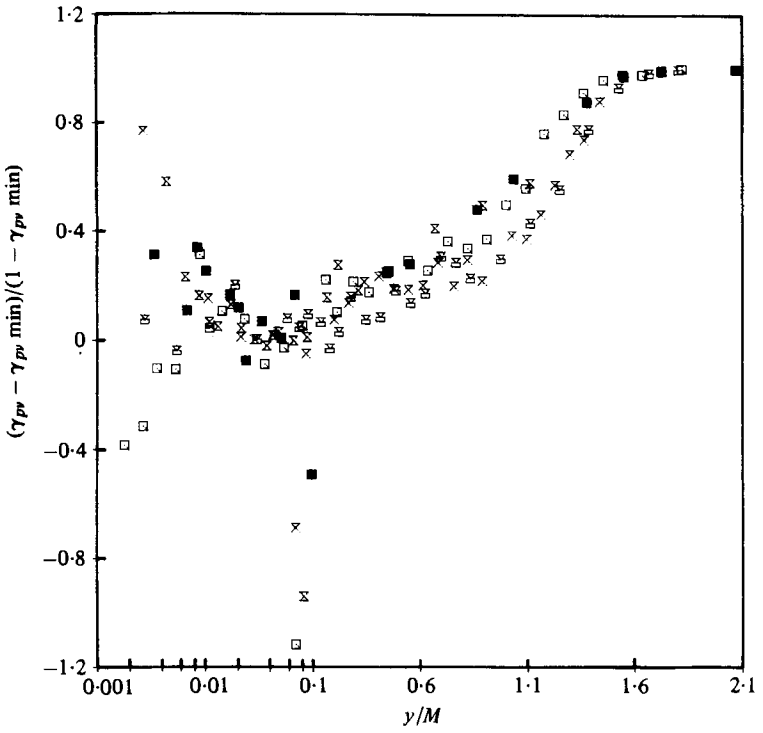

FIGURE 12. $(\gamma_{pv}-\gamma_{pv\min})/(1-\gamma_{pv\min})$ *vs.* y/M; $M = y$ at $v'_{\max}$. Data: ⧖, 134·5 in.; ■, 138·8; ⧖, 144·9; ◱, 156·4; ⧗, 170·9.

In describing a quantitative amount of backflow, the word 'detachment' was preferred over 'separation' since the latter term refers to the entire phenomenon. Here we shall continue to use the time-honoured terminology as well as the new terminology.

Downstream of intermittent separation, Simpson *et al.* (1977) showed the existence of similarity in γ_{pu} distributions by normalizing and plotting $(\gamma_{pu}-\gamma_{pu0})/(1-\gamma_{pu0})$ *vs.* y/M where γ_{pu0} was taken as the value near the wall as obtained from a figure similar to figure 6 and M was the distance of the peak in the u' distribution from the wall. The present data also exhibit similarity, particularly in the region $0{\cdot}1 \leqslant y/M \leqslant 1{\cdot}0$, with it improving as one moves downstream. In fact the last two stations at 156·4 in. and 170·9 in. show the similarity existing across all the boundary layer, including the backflow region. The similarity in the backflow region improves when the minimum value of γ_{pu} is used instead of γ_{pu0} as shown in figure 11. This is due to the relatively large uncertainty in γ_{pu0}. Simpson *et al.* (1977) fitted a curve to their data and gave an equation for the distribution in the region $0{\cdot}1 \leqslant y/M \leqslant 1{\cdot}0$. Figure 11 shows that the present data approximately satisfy the equation. Similar plots drawn with M being taken as the distance from the wall to the location where peaks were observed in the v' and $-\overline{uv}$ distributions show as good or better similarity.

Similarity profiles also exist for γ_{pv} or the fraction of time that the flow is away from the wall. Because the uncertainties in γ_{pv} are relatively large near the wall, $\gamma_{pv\min}$ was used in the normalized results shown in figure 12 for the region downstream of intermittent separation. Near the outer edge of the boundary layer the intermittency is everywhere approximately equal to one, indicating that the flow is always

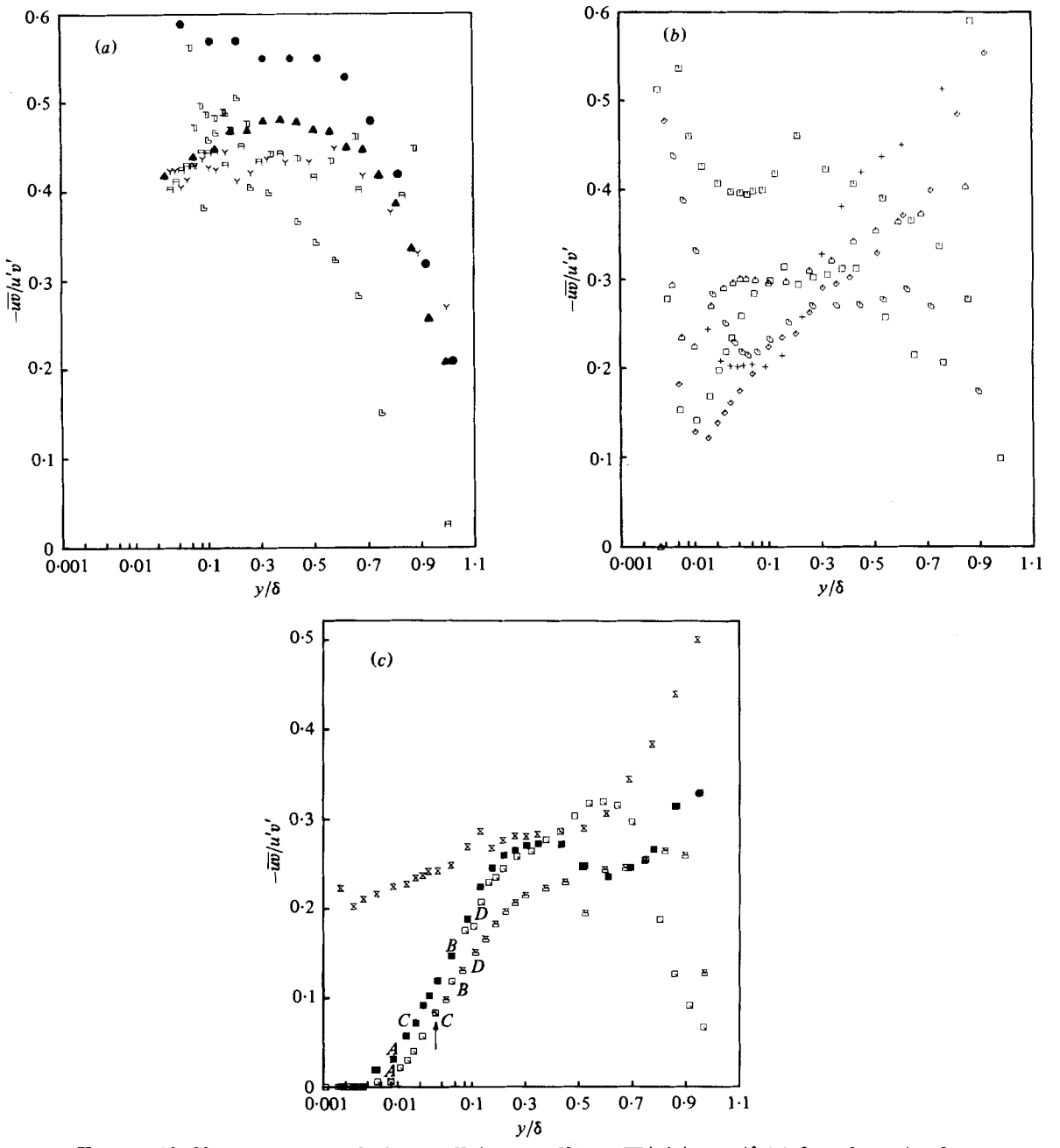

FIGURE 13. Shear stress correlation coefficient profiles $-\overline{uv}/u'v'$ *vs.* y/δ (*a*) from hot-wire data upstream from separation, (*b*) from smoothed laser and hot-wire data in the vicinity of the beginning of intermittent backflow, and (*c*) from smoothed laser and hot-wire data in the separated flow region. (*a*) Schubauer & Klebanoff (1951): ●, near the beginning of the deceleration, 17·5 ft; ▲, 22·5 ft. Data ⊔, 31·7 in.; ▯, 64·2; ⊓, 86·5; Y, 105·3. (*b*) ▯, 112·4 in.; ◔, 118·5; ⌂, 120·5; +, 122·6; ◈, 129·4; □, 131·9. (*c*) ⧗, 134·5 in.; ■, 138·8; ⊔, 144·8; ◪, 156·4. Letters *A–D* denote turbulence profile inflection points noted by Shiloh *et al.* (1981). The arrow denotes the location of the minimum mean velocity. Note the log-linear abscissa.

directed outwards. Near the wall, the intermittency γ_{pv} obtained in the region downstream of intermittent separation is higher than the values attained upstream of it, which can be attributed to the flow leaving the wall as a consequence of intermittent separation. As in the case of γ_{pu}, the distributions near the wall are trough-shaped in the region downstream of intermittent separation and show some similarity.

5.3. *Turbulence correlations*

(*a*) *Reynolds stresses correlations.* Figure 13 shows distributions of the shear-stress correlation coefficient $-\overline{uv}/u'v'$, which is a measure of the extent of correlation between u and v fluctuations. In the middle part of the boundary layer $-\overline{uv}/u'v'$ is about $\pm 19\%$ uncertain. Near the outer edge the values are much more uncertain since $-\overline{uv}$, u' and v' approach zero. Figure 13(*a*) also shows distributions for the Schubauer & Klebanoff (1951) strong-adverse-pressure-gradient boundary layer. These two sets of measurements compare reasonably well, even though the adverse-pressure-gradient distributions are different.

Figure 13(*b*) shows distributions in the vicinity of the beginning of intermittent backflow. Unlike the distributions far upstream shown in figure 13(*a*) or those observed in zero-pressure-gradient boundary layers, the distributions in this region do not exhibit a constant value over a large part of the outer layer. However, the distributions for some of the stations do indicate a small region with a nearly constant value as low as 0·2 to 0·3. As one moves downstream, the peaks for the distributions seem to move gradually towards the outer edge of the boundary layer. Similar features such as correlation coefficients as low as 0·3 with the peaks occurring near the outer edge of the boundary layer were observed by Spangenberg, Rowland & Mease (1967) in their experiments on an adverse-pressure-gradient flow approaching separation. Figure 13(*c*) indicates that the profiles for the separated region seem to exhibit some similarity.

Simpson *et al.* (1980) give the distributions of another type of correlation coefficient, $a_1 = -\overline{uv}/(u'^2+v'^2)$. In the middle part of the boundary layer a_1 is about $\pm 20\%$ uncertain. Like $-\overline{uv}/u'v'$, near the outer edge a_1 is much more uncertain since $-\overline{uv}$, u', and v' approach zero. Upstream of separation, a_1 is in reasonable agreement with the data of East & Sawyer (1979) for favourable and adverse-pressure-gradient flows. Considering the wide variations in the flow conditions and the uncertainties in the measurements, the agreement seems to be reasonable, particularly for the adverse-pressure-gradient case. The variation in the behaviour of the distributions as one moves downstream is similar to that for the shear correlation coefficient $-\overline{uv}/u'v'$, with an increasingly reduced flat region and a reduction in the value of a_1 to as low as 0·1 for the separated region. Shiloh *et al.* (1981) present $-\overline{uv}/(u'^2+v'^2+w'^2)$ distributions for this flow.

(*b*) *Eddy viscosity and Prandtl mixing-length distributions.* The Prandtl mixing length

$$\frac{l}{\delta} = \frac{(-\overline{uv})^{\frac{1}{2}}}{\delta}\left|\frac{\partial U}{\partial y}\right|^{-\frac{1}{2}}\left(\frac{\partial U}{\partial y}\right)^{-\frac{1}{2}} \tag{10}$$

and the eddy viscosity

$$\frac{\nu_e}{U_\infty \delta_1} = \frac{-\overline{uv}}{U_\infty \delta_1 \partial U/\partial y} \tag{11}$$

were calculated from measured Reynolds shearing stress and calculated velocity

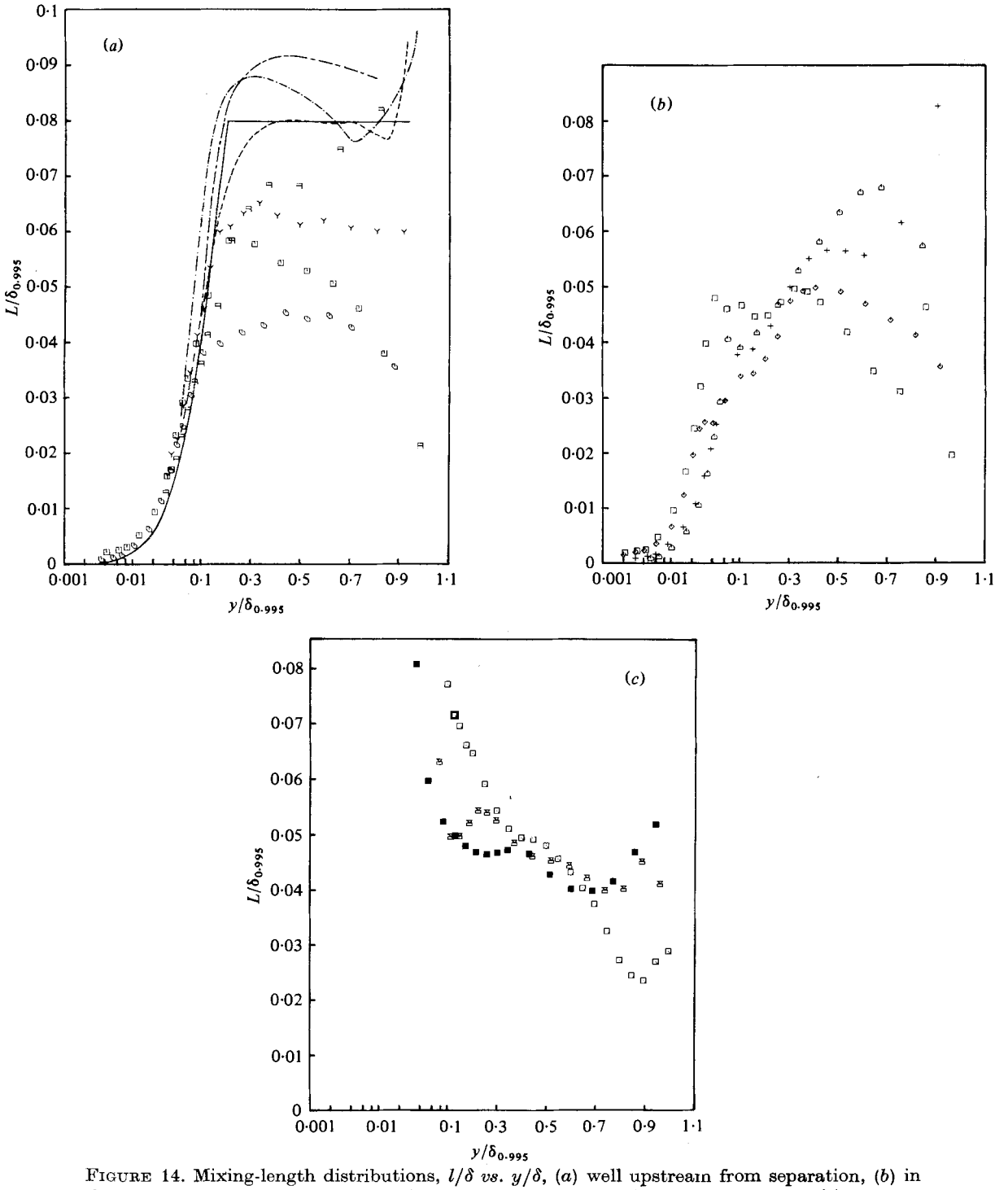

FIGURE 14. Mixing-length distributions, l/δ *vs.* y/δ, (*a*) well upstream from separation, (*b*) in the vicinity of separation, and (*c*) downstream from separation. (*a*) ⊟, 86·5 in.; ⋎, 105·25; ⊡, 112·4; ◹, 118·5. Bradshaw (1967) – – – –, $a = -0{\cdot}15$ flow; —·—, $a = -0{\cdot}225$ flow. East & Sawyer (1979): — — —, flow 4. Cebeci & Smith (1974) (van Driest) ——. Note the log-linear abscissa. (*b*) ⏢, 120·5 in.; +, 122·6; ◈, 129·4; □, 131·9. (*c*) ■, 138·75 in.; ⧈, 144·9; ◹, 156·4.

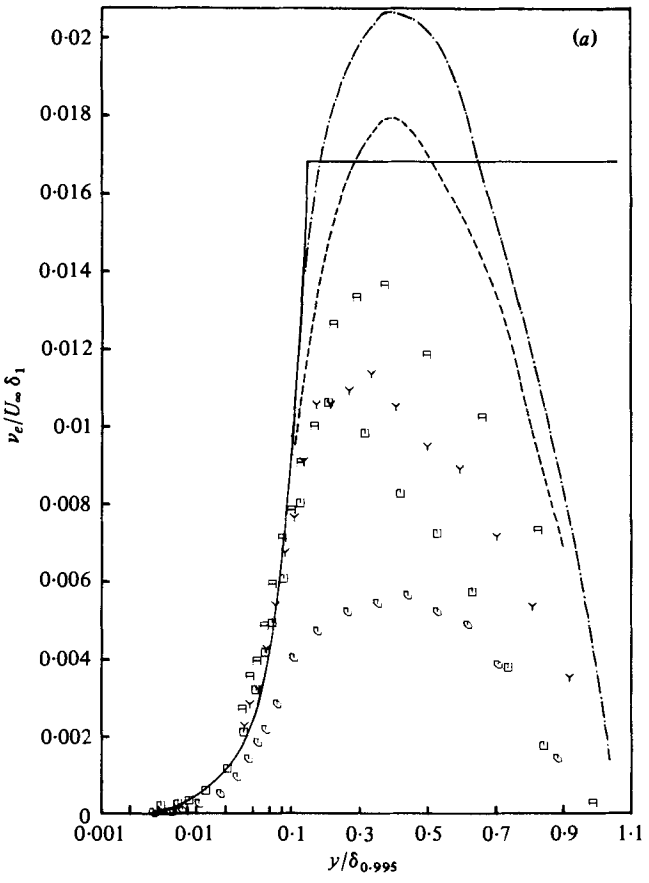

FIGURE 15. Eddy viscosity distributions, $\nu_c/U_\infty\delta_1$, (*a*) well upstream from separation, (*b*) in the vicinity of separation, and (*c*) downstream from separation. (*a*) ⊟, 86·5 in.; Y, 105·25; ⊡, 112·4; ◹, 118·5. Bradshaw (1967): – – – –, $a = -0{\cdot}15$ flow; —·—, $a = -0{\cdot}255$ flow. Cebeci (1974) (van Driest) ——. Note the log-linear abscissa. (*b*) ⏢, 120·5 in.; +, 122·6; ◇, 129·4; □, 131·9. (*c*) ■, 138·75 in.; ⧉, 144·9; ◲, 156·4.

gradient distributions. From the near-wall region to the middle of the boundary layer, the hot-wire mixing-length and eddy-viscosity results are about $\pm 20\,\%$ uncertain while the LDV results are about $\pm 12\,\%$ uncertain. In the outermost part of the boundary layer the results are much more uncertain since $-\overline{uv}$ and $\partial U/\partial y$ approach zero. As shown by Simpson *et al.* (1980), the mixing-length results upstream of the throat of the test section are in good agreement within the limits of uncertainty with the zero-pressure-gradient results of Klebanoff (1955) and the zero- and favourable-pressure-gradient results of East & Sawyer (1979).

Figure 14(*a*) covers the adverse-pressure-gradient region of the flow up to the start of incipient detachment. The data of Bradshaw (1967) for adverse-pressure-gradient equilibrium boundary layers and East & Sawyer (1979) are presented for comparison. Also shown is Cebeci & Smith's (1974) extension of van Driest's mixing-length model for the inner layer,

$$l = 0{\cdot}4y(1-\exp(-y/A)), \quad A = \frac{26\nu}{U_\tau N}, \quad N = (1-11{\cdot}8p^+)^{\frac{1}{2}}, \quad p^+ = \frac{\nu U_\infty}{U_\tau^3}\frac{dU_\infty}{dx} \tag{12}$$

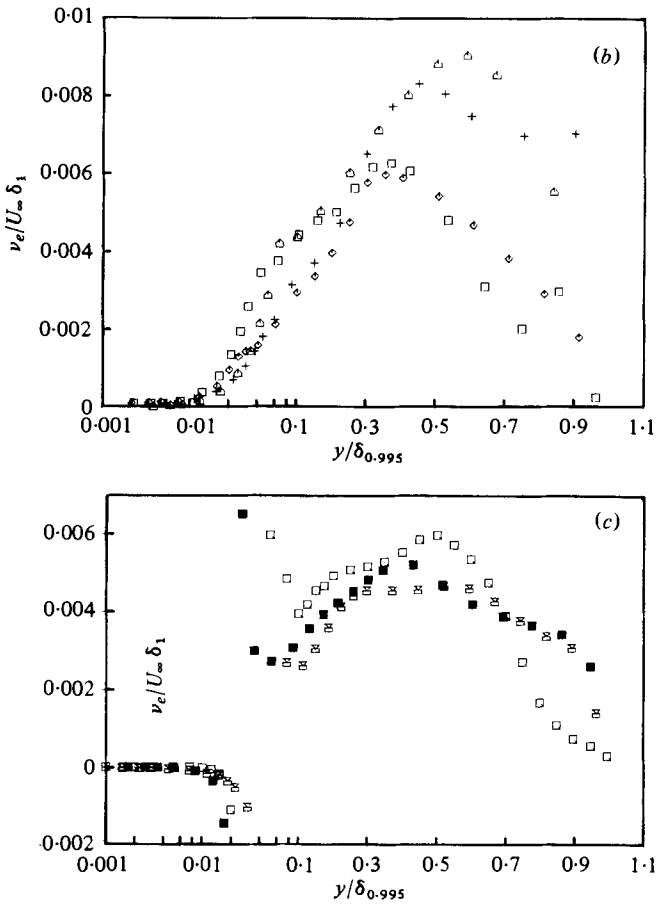

FIGURE 15*b*, *c*. For legend see p. 45.

for the 86·5 in. location. A constant value of 0·08 is used for l/δ in the outer region. The present data at 86·5 in. are in reasonable agreement with these results.

Although the downstream stations exhibit similarity in the inner layer, they show a continuously decreasing mixing length in the outer layer as one moves downstream. Further downstream in the intermittent separation region, the inner layer similarity gradually disappears and the mixing length in the outer layer continues to decrease with no region of constant mixing length. In the separated region, Prandtl's mixing length cannot be defined in the backflow region where $\partial U/\partial y$ is negative. The distributions for the forward flow region are shown in figure 14(*c*). They indicate large values of the mixing length closest to the wall where it can be defined, decreasing continuously as one moves farther away from the wall. There is also some indication of the profiles achieving similarity.

Figure 15 shows the eddy viscosity profiles in the various regions. As in the case of the mixing length, a few sets of data from earlier investigations are also plotted for comparison. In general, the same comments made about the mixing-length profiles are applicable to these profiles also. The present data near the test section throat show good agreement with Klebanoff's (1955) zero-pressure-gradient data. The data in figure 15(*a*) show good agreement with Bradshaw's data in the adverse-pressure-

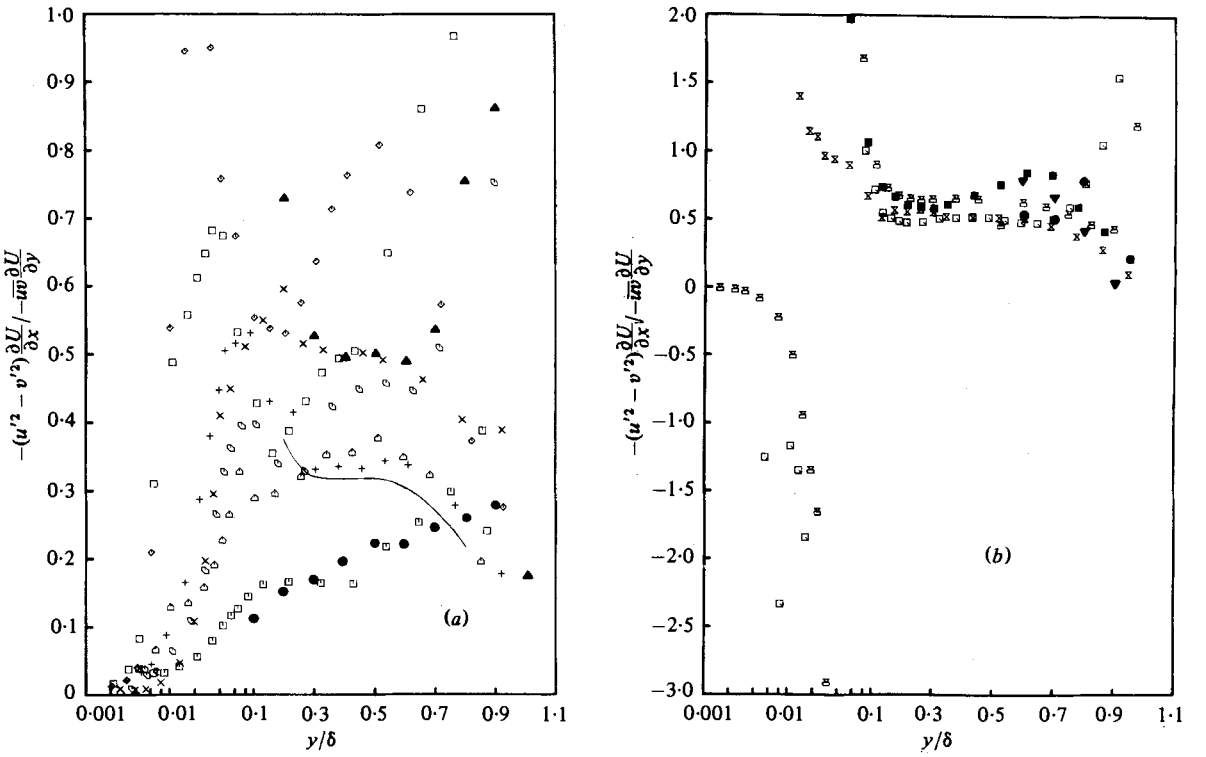

FIGURE 16. Ratio of normal stresses production to shear-stress production (*a*) upstream and (*b*) downstream from separation. (*a*) ⊡, 112·4 in.; ◌, 118·5; ⌓, 120·0; +, 122·6; ×, 127·1; ◇, 129·1; □, 131·9. Schubauer & Klebanoff (1951) ——, near separation. Simpson *et al.* (1977): ●, 103·8 in.; ▲, 124·3. Note the log-linear abscissa. (*b*) ⧖, 134·5 in.; ■, 138·75; ⧖, 144·9; ◻, 156·4. Simpson *et al.* (1977) ▼, 139·1 in.; ●, 157·1.

gradient region in the inner layer. A prediction using Cebeci and Smith's model in the relation

$$\nu_e = l^2 \frac{\partial U}{\partial y} \tag{13}$$

is in reasonable agreement with the inner layer data at 86·5 in.

At first it is a little surprising that there is similarity in the inner layer mixing-length distributions and similarity in the inner layer eddy viscosity distributions near separation when δ is used for scaling y. However, the ratio of $U_\tau \delta$ at successive stations is near unity in this region, so $y^+/(y/\delta)$ is the same for successive stations and the profiles near the wall are similar with respect to y^+ as well. In the intermittent separation region, the inner layer similarity disappears and the eddy viscosity decreases with respect to x in the outer layer. In the separated region, ν_e can be defined everywhere except where $\partial U/\partial y = 0$. Eddy viscosity profiles also show some similarity in the outer layer as well as near the wall in the separated region.

For both mixing length and eddy viscosity, the data in the vicinity of separation indicate much lower values in the outer region than for attached boundary layers. This is understandable since part of the momentum transport is due to normal stresses. As shown below, normal stresses effects can be used to explain this behaviour.

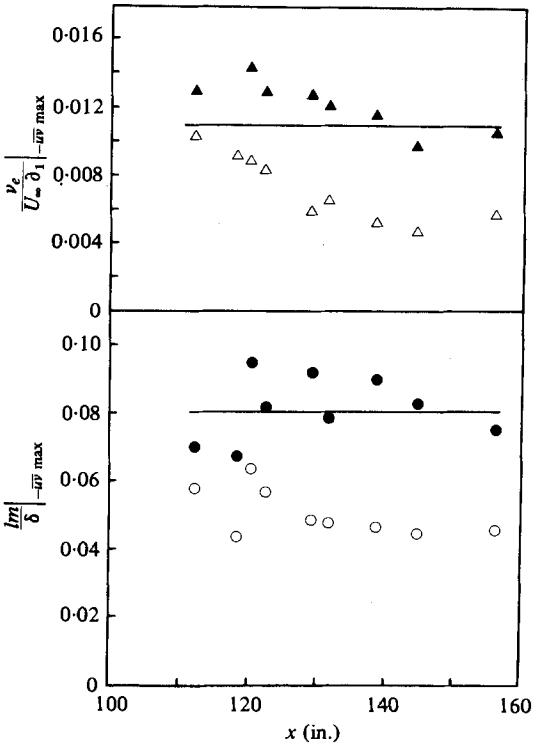

FIGURE 17. $\nu_e/U_\infty\delta_1$ and l_m/δ at the maximum shearing stress location. Open symbols represent experimental data; ▲, correlation using equation (16); ●, correlation using equation (15); ——, flat-plate boundary layer with $F = 1$.

5.4. *Effects of normal stresses on mixing length and eddy viscosity*

As noted in the earlier work of Simpson *et al.* (1977), the normal stresses turbulence energy production terms are important in separating flows. Simpson *et al.* defined a non-dimensional factor F as the ratio of total turbulence energy production to the shear-stress-related turbulence energy production

$$F = 1 - \frac{(u'^2 - v'^2)\,\partial U/\partial x}{-\overline{uv}\,\partial U/\partial y}. \tag{14}$$

Figure 16 shows $F-1$ for the several locations in the vicinity of separation. As indicated by the present data and the data of Simpson *et al.* (1977) and Schubauer & Klebanoff (1950), the normal stresses effect becomes increasingly important as separation is approached. In fact both sets of data from Southern Methodist University show good agreement in the corresponding regions of development, with a near doubling of the ratio in the intermittent separation region. The present data in that region indicate the presence of a hump in the distributions near y/δ of 0·05 to 0·1, which becomes more significant as separation is approached. This is a result of the mean velocity profiles becoming inflexional in nature, which produces a reduced $\partial U/\partial y$ in that region. In fact these humps increase rapidly along the flow until $\partial U/\partial y$ attains a zero value for each profile in the backflow region where the velocity reaches a minimum value. The earlier data of Simpson *et al.* (1977) at 124·3 in. also suggest the

presence of a hump. In the backflow region the two types of production oppose each other as shown in figure 16(*b*), but they aid one another in the forward flow region. The distributions in the outer layer tend toward similarity and the ratio seems to be almost a constant of 0·6 for $0{\cdot}2 \leqslant y/\delta \leqslant 0{\cdot}7$.

As shown in figures 14 and 15, the mixing-length and eddy viscosity distributions in the outer region decrease in magnitude in the downstream direction. This seems to be consistent with Gartshore's (1967) suggestion of decreased Reynolds shear stress in flows with an extra strain rate $\partial V/\partial y$, as in his own experiments on retarded wakes. Figures 17(*a*, *b*) show these parameters at the maximum shearing stress for each location. F was fitted to these data with the following results:

$$\frac{l}{\delta} = \left(\frac{1}{F^{1{\cdot}25}}\right)\frac{l}{\delta}\bigg|_{F=1} \tag{15}$$

and

$$\frac{\nu_e}{U_\infty \delta_1} = \left(\frac{1}{F^{1{\cdot}5}}\right)\frac{\nu_e}{U_\infty \delta_1}\bigg|_{F=1}. \tag{16}$$

These results were obtained in the following manner. The normally accepted value of 0·08 was used for l/δ at $F = 1$. Using this, an average value for l/δ in the outer region, and the value of F at the location of the maximum shearing stress, the exponent on F in equation (15) was determined at each streamwise location. This exponent was within 12 % of 1·25 and the modified correlation $F^{1{\cdot}25}l/\delta$ agrees within the limits of experimental uncertainty of 21 % with the normally accepted value of 0·08.

For evaluating the exponent in equation (16), all values were taken at the location of the maximum shearing stress; 105·3 in. was considered the location where $F = 1$. Equation (16) agrees with the data within the uncertainty of 26 %.

6. Conclusions – the nature of a separating turbulent boundary layer

These experiments confirm the conclusions of Simpson *et al.* (1977) regarding a separating-airfoil-type turbulent boundary layer. The mean flow upstream of the beginning of intermittent separation obeys the law of the wall and the Perry & Schofield (1973) velocity profile correlation for the outer region. The correlations of Sandborn & Liu for the locations of intermittent separation ($\gamma_{pu} = 0{\cdot}8$) and fully developed separation hold. Pressure gradient relaxation begins upstream of intermittent separation near the wall jet control in this flow and continues until the location of fully developed separation. The upstream–downstream intermittency γ_{pu}, u', v' and $-\overline{uv}$ profiles each approach similarity profiles downstream of separation.

Much new information about the separated region has been gathered and leads to significant conclusions about the nature of the separated flow. For reference the most important results are summarized below.

(1) The backflow mean velocity profile scales on the maximum negative mean velocity U_N and its distance from the wall N. A U^+ *vs.* y^+ law-of-the-wall velocity profile is not consistent with this correlation since both U_N and N increase with streamwise distance, while the law-of-the-wall length scale ν/U_τ varies inversely with the velocity scale U_τ. It does not appear possible to describe the separated flow mean velocity profiles by a universal 'backflow function' that is added to a universal 'wake function'.

(2) High turbulence levels exist in the backflow. u' and v' are of the same order as $|U|$. Since the free-stream velocity in the separated region is rather steady, this means that the near wall fluctuations are not due mainly to a flapping of the entire shear layer, but are due to turbulence within the separated shear layer.

(3) Low levels of Reynolds shearing stress occur in the backflow. $-\overline{uv}/u'v'$ and $-\overline{uv}/(u'^2+v'^2)$ correlations are very low in the backflow.

(4) $-\overline{uv}/u'v'$ and $-\overline{uv}/(u'^2+v'^2)$ correlations are about 25% lower in the outer region of the separated flow than for the upstream attached flow.

(5) Mixing-length and eddy viscosity models are adequate upstream of separation and in the outer region, but are physically meaningless in the backflow. Normal stresses effects appear to account for the lower mixing-length and eddy viscosity values observed in the outer region of the separated flow.

Downstream of fully developed separation in these experiments, the mean backflow region appears to be divided into three layers: a viscous layer nearest the wall that is dominated by the turbulent flow unsteadiness but with little Reynolds shearing-stress effect; a rather flat intermediate layer that seems to act as an overlap region between the viscous wall and outer regions; and the outer backflow region that is really part of the large-scaled outer region flow.

The Reynolds shearing stresses in this region must be modelled by relating them to the turbulence structure and not to the local mean velocity gradients. The mean velocity profiles in the backflow are a result of time-averaging the large turbulent fluctuations and are not related to the cause of the turbulence. In contrast, in flows for which the eddy viscosity and mixing-length models appear to be useful, the instantaneous velocity gradients are not extremely different from the local mean velocity gradient, i.e. the Reynolds shearing stress is physically related to the mean velocity gradient.

This work was supported by Project SQUID, an Office of Naval Research Program.

REFERENCES

Bradshaw, P. 1967 *J. Fluid Mech.* **29**, 625–645.

Bradshaw, P., Ferriss, D. H. & Atwell, N. P. 1967 *J. Fluid Mech.* **28**, 593–616.

Bragg, G. M. 1974 *Principles of Experimentation and Measurement.* Prentice-Hall.

Cebeci, T., Khalid, E. E. & Whitelaw, J. H. 1979 *A.I.A.A. J.* **17**, 1291–1292.

Cebeci, T. & Smith, A. M. O. 1974 *Momentum Transfer in Boundary Layers.* Hemisphere.

Coles, D. & Hirst, E. 1969 *Computation of Turbulent Boundary Layers* - 1968 *AFOSR-IFP Stanford Conf. Vol.* II, *Data Compilation.* Dept Mechanical Engng, Stanford Univ.

Coles, D. & Wadcock, A. 1979 *A.I.A.A. J.* **17**, 321–329.

Collins, M. A. & Simpson, R. L. 1978 *A.I.A.A. J.* **16**, 291–292.

Durão, D. F. G. & Whitelaw, J. H. 1975 *Proceedings of LDA Symposium Copenhagen*, pp. 138–149. P.O. Box 70, DK – 2740 Skovlunde, Denmark.

East, L. F. & Sawyer, W. G. 1979 *Proc. NATO-AGARD Fluid Dynamics Symp.*

Gartshore, I. S. 1967 *J. Fluid Mech.* **30**, 547–560.

Higuchi, H. & Peake, D. J. 1978 *N.A.S.A. Tech. Memo* 78531.

Klebanoff, P. 1954 *N.A.C.A. Rep.* 1247.

Kline, S. J. & McClintock, F. A. 1953 *Mech. Engng* **75**, 3–8.

McLaughlin, K. D. & Tiederman, W. G. 1973 *Phys. Fluids* **16**, 2082–2088.

Miller, J. A. 1976 *Trans. A.S.M.E.* I, *J. Fluids Engng* **98**, 550–557.

MURTHY, V. W. & ROSE, W. C. 1978 *A.I.A.A. J.* **16**, 667–672.

OKA, S. & KOSTIĆ, Z. 1972 *DISA Information*, no. 13, pp. 29–33.

PERRY, A. E. & SCHOFIELD, W. H. 1973 *Phys. Fluids* **16**, 2068–2074.

PLETCHER, R. H. 1978 *Trans. A.S.M.E.* I, *J. Fluids Engng* **100**, 427–433.

RUBESIN, M. W., OKUNO, A. F., MATEER, G. G. & BROSH, A. 1975 *N.A.S.A. Tech. Memo.* X-62, 465.

SANDBORN, V. A. & KLINE, S. J. 1961 *Trans. A.S.M.E.* D, *J. Basic Engng* **83**, 317–327.

SANDBORN, V. A. & LIU, C. Y. 1968 *J. Fluid Mech.* **32**, 293–304.

SCHUBAUER, G. B. & KLEBANOFF, P. S. 1951 *N.A.C.A. Rep.* 1030.

SHILOH, K., SHIVAPRASAD, B. G. & SIMPSON, R. L. 1981 *J. Fluid Mech.* **113**, 75–90.

SHIVAPRASAD, B. G. & SIMPSON, R. L. 1981 *Trans. A.S.M.E.* I, *J. Fluids Engng* (accepted).

SIMPSON, R. L. 1976 *A.I.A.A. J.* **14**, 124–126.

SIMPSON, R. L. 1979 *Trans. A.S.M.E.* I, *J. Fluids Engng* (to appear). (Also Project SQUID Rep. SMU-3-PU.)

SIMPSON, R. L. & BARR, P. W. 1975 *Rev. Sci. Instrum.* **46**, 835–837.

SIMPSON, R. L. & CHEW, Y.-T. 1979 *Proceedings of Third Int. Workshop on Laser Velocimetry*, pp. 179–196. Hemisphere.

SIMPSON, R. L., CHEW, Y.-T. & SHIVAPRASAD, B. G. 1980 Project SQUID Rep. SMU-4-PU. (To appear as DTIC or NTIS Report.)

SIMPSON, R. L., CHEW, Y.-T. & SHIVAPRASAD, B. G. 1981 *J. Fluid Mech.* **113**, 53–73.

SIMPSON, R. L. & COLLINS, M. A. 1978 *A.I.A.A. J.* **16**, 289–290.

SIMPSON, R. L., HEIZER, K. W. & NASBURG, R. E. 1979 *Trans. A.S.M.E.* I, *J. Fluids Engng* **101**, 381–382.

SIMPSON, R. L., STRICKLAND, J. H. & BARR, P. W. 1974 Thermal and Fluid Sciences Center, Southern Methodist Univ., Rep. WT-3; also AD-A001115.

SIMPSON, R. L., STRICKLAND, J. H. & BARR, P. W. 1977 *J. Fluid Mech.* **79**, 553–594.

SPANGENBERG, W. G., ROWLAND, W. R. & MEASE, N. E. 1967 *Fluid Mechanics of Internal Flow* (ed. G. Sovran), pp. 110–151. Elsevier.

STRICKLAND, J. H. & SIMPSON, R. L. 1973 *Thermal and Fluid Sciences Center, Southern Methodist Univ.*, Rep. WT-2; also AD-771170/8GA.

WOOD, N. B. 1975 *J. Fluid Mech.* **67**, 769–786.